Paper

Torsional Vibration Characteristics Analysis of DFIG-based Wind Farm and Its Equivalent Model Research

Da Xie*a), Non-Member
Junbo Sun*, Non-Member
Yupu Lu*, Non-Member
Yucheng Lou*, Non-Member
Chenghong Gu**, Non-Member
Furong Li**, Non-Member

As large-scale wind farms (WFs) are integrated to the power grid, the interaction between the WF and the grid may excite shaft torsional vibration of the wind turbine. To study the shaft torsional vibration characteristics of the doubly fed induction generator (DFIG)-based WF, a detailed small signal model for DFIG is established first. Then the small signal model for a WF composed of multi-DFIGs is developed on the basis of the single-machine model. Modal analysis is employed to investigate the torsional vibration characteristics of a WF made up of several identical DFIGs, whose accuracy is also demonstrated through the time-domain simulation. To simplify the torsional vibration analysis for the DFIG-based WF, a reduced order equivalent model is proposed. The results obtained from modal analysis show that the equivalent model not only precisely maintains all the torsional vibration modes of the original small-signal model, but also greatly reduces the computation complicity. With the equivalent model, the "dimension disaster" problem is solved in torsional vibration analysis for large WFs, which is of great help in further damping schemes design.

Keywords: Doubly Fed Induction Generator (DFIG), equivalent model, shaft torsional vibration, small signal analysis, wind farm.

1. Introduction

As a green and renewable energy resource, wind energy has been developed quickly in recent years, which has led to the explosive growth of wind turbine generators (WTGs) connected to the power grid [1, 2]. However, there also exist obvious disadvantages of wind energy, such as intermittency of wind. Thus, the large amount of WTGs integrated to the grid will impact the power system a lot (e.g. low-~~—~~frequency oscillation and sub-synchronous oscillation (SSO) etc.), which will, in turn, ~~in turn~~ excite shaft torsional vibration of wind turbines [3]. The torsional vibration may reduce the lifespan of the wind turbine, and the even worse case is resulting in shaft break [4]. Therefore, it is of great significance to study the torsional vibration characteristics of WTGs, especially that of large Wind farms (WFs).

To achieve a high conversion efficiency of wind energy, various speed wind turbines are in wide adoption. Among a~~the~~ large number of variable speed wind turbines, doubly-fed induction generator (DFIG)-based wind turbine is popularly used nowadays for its high power efficiency, economical characteristic, and power decoupling controllability [5-7]. There exist a multitude of literature~~s~~ on DFIG modeling and dynamic characteristics analysis of DFIG-based wind turbines. An available model of DFIG is developed in [8] to study how the model parameters will influence the transient responses of DFIG-based wind plants. But the mechanical system and electrical system are both simplified during the investigation. Thus, the dynamic characteristics of the shaft cannot be analyzed in detail. Reference [9, 10] use the modal analysis to characterize the small-signal behavior of DFIG wind turbine, and research the DFIG intrinsic dynamics with the change of the system parameters, operating points, grid strength and some other factors, which neglects the shaft torsion vibration during the research. To reflect the dynamic characteristics of the shaft, reference [11-13] developed a lump shaft model, a two-mass model and a three-mass shaft model for the drive train of DFIG respectively. The simulation results show that when the drive train is modeled with more masses, the dynamic characteristics of the shaft system can be analyzed more clearly and accurately. It is noted that above researches are concentrated on the dynamic characteristics of a single DFIG, and that of a large WF is not involved, especially the shaft torsional vibration.

With the size of WFs increasing, the wind turbines will influence each other greatly during operation. A s~~S~~mall disturbance in the WF may impact the power grid greatly, such as low-~~—~~frequency oscillation and even system splitting. Also, electrical disturbance (e.g. voltage sag) may excite shaft torsional vibration in one or several WTGs when the damping is at a low level. So it is necessary to study the dynamic characteristics of WFs and the research topic is gaining increasing interests. Reference [14] developed an equivalent model for the fixed speed induction generator (FSIG) WF. During the research, the drive train is modeled with only one mass, which fails to analyze the dynamic characteristic of the shaft clearly. The small-signal model of a WF is developed in [15] to research the effect of series

a) Correspondence to: Da Xie. E-mail: profxzg@hotmail.com
* Department of Electrical Engineering, Shanghai Jiao Tong University, Shanghai, China
** Department of Electronic & Electrical Engineering, University of Bath, Bath, UK

compensation capacitor on torsional vibration, while the gear box is represented with the ratio and the shaft system is modeled with just two masses. In [16], the two-mass shaft model is also adopted for the FSIG WF to study the effect of different system parameters on fault-clearing time. However, the torsional vibration between different wind turbines is ignored in the aforementioned literatures since the WF is equivalent to one unit or the mechanical system is not modeled in detail. Also, how will the number of wind turbines influence the torsional vibration of the WF is not researched, either. Another problem is that when the WTGs of a WF are all modeled with differential equations, the state matrix will be in high dimension and difficult or impossible to deal with. Then a valid equivalent model for a WF is necessary to study its dynamic characteristics.

In order to exactly analyze the torsional vibration characteristics of the mechanical system of DFIG, a three-mass shaft model, which consists of blades, a gearbox, a low-speed shaft, a high-speed shaft and an induction generator rotor in [17] is adopted. Then the small signal model of the voltage source converter (VSC) is developed, where the three subsystems, including a rotor side converter (RSC), a grid side converter (GSC) and a DC-link, are modeled respectively. The transmission line and the transformer are modeled as an equivalent RLC (resistor, inductor and capacitor) line. At last, the union small signal model of DFIG consisting of seven modules is obtained. Based on the model of a single DFIG, the small signal model of a DFIG-based WF is derived. Through conducting matrix transformation to the state matrix of the WF model, an equivalent model for the WF is proposed and its accuracy is validated through eigenvalues analysis.

The novelty of this paper is that it: i) develops a small signal model of DFIG-based wind power system for easy shaft torsional vibration analysis; ii) establishes a small signal model for a WF and study its shaft torsional vibration through modal analysis; iii) propose an effective equivalent model for shaft torsional vibration analysis of WF, which reduces the computation complexity significantly.

The remaining parts of this paper are organized as follows. Section 2 provides the union small-signal model of the DFIG, consisting of the drive train, the induction generator, the converter controller and the transmission line model. An equivalent model for WF to simplify the torsional vibration analysis is proposed in Section 3. Section 4 employs the modal analysis to study the shaft torsional vibration issues of DFIG-based WF with identical WTGs and the results are demonstrated through time domain simulation. Finally, conclusions are drawn in section 5.

2. Model of grid-connected DFIG wind turbine

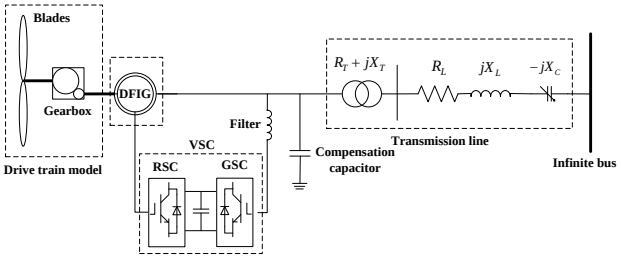

Fig.1 Schematic diagram of the DFIG wind turbine

The schematic diagram of the studied DFIG-based wind turbine is shown in Fig.1 [18]. The wind turbine is connected to the induction generator via a gearbox. The stator side of the induction generator is connected to the infinite bus by a transmission line, including the impedance of transformer and cable. The rotor side is fed through a VSC and a filter to supply exciting voltage to the induction generator, where the inductor is used as a filter. The compensation capacitor is used to provide reactive power for the DFIG. As shown in Fig.1, the model of the grid-connected DFIG wind turbine mainly consists of five parts: the drive train, DFIG, VSC, filter and the transmission line.

2.1 Three-mass drive train model The mechanical system of a wind turbine is composed of windmill blades, a low-speed shaft, a gearbox, a high-speed shaft and the generator rotor. All the shaft parts can be lumped into masses to describe the physical characteristics of the real system. To study the drive train system accurately, a three-mass shaft model in [17] is adopted shown in Fig.2.

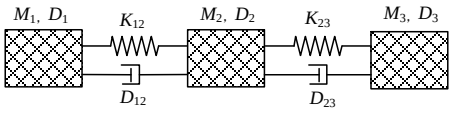

Fig.2 Three-mass drive train model for DFIG

The three-mass drive train model can be expresseds as

$$\begin{cases} M_1\dfrac{d\omega_{rot}}{dt} = T_w - K_{12}(\theta_1-\theta_2) - D_1\omega_{rot} - D_{12}(\omega_{rot}-\omega_2) \\ M_2\dfrac{d\omega_2}{dt} = -K_{12}(\theta_2-\theta_1) - K_{23}(\theta_2-\theta_3) - D_2\omega_2 - D_{12}(\omega_2-\omega_{rot}) \\ \qquad\qquad - D_{23}(\omega_2-\omega_{gen}) \\ M_3\dfrac{d\omega_{gen}}{dt} = -T_e - K_{23}(\theta_3-\theta_2) - D_3\omega_{gen} - D_{23}(\omega_{gen}-\omega_2) \\ \dfrac{d\theta_1}{dt} = \omega_{rot} \\ \dfrac{d\theta_2}{dt} = \omega_2 \\ \dfrac{d\theta_3}{dt} = \omega_{gen} \end{cases} \tag{1}$$

where, M_1, M_2 and M_3 denote the moment of inertia of the blades, low speed shaft and the high speed shaft respectively; ω_{rot}, ω_2 and ω_{gen} denote the angular velocity of the three parts respectively; θ_1, θ_2 and θ_3 are mechanical rotation angle of the three parts respectively; D_1, D_2 and D_3 are damping coefficient of the three parts respectively and D_{12} the damping coefficient between the blades and the low-speed shaft and D_{23} the damping coefficient between the low and high-speed shaft; K_{12} and K_{23} are torsional stiffness of the low-speed and high-speed shafts respectively; T_w is input wind torque from the blade side; T_e is the electromagnetic torque of the generator.

After linearizing equation (1), the corresponding small signal model for the three-mass drive train is presented as follows:

$$\begin{cases} \dot{X}_{DT} = A_{DT} X_{DT} + B_{DT} u_{DT} \\ Y_{DT} = C_{DT} X_{DT} + D_{DT} u_{DT} \end{cases} \tag{2}$$

where subscript *DT* denotes the three-mass drive train model, and

$X_{DT} = \begin{bmatrix} \Delta\theta_1 & \Delta\theta_2 & \Delta\theta_3 & \Delta\omega_{rot} & \Delta\omega_2 & \Delta\omega_{gen} \end{bmatrix}^T$;

$Y_{DT} = \begin{bmatrix} \Delta\theta_3 & \Delta\omega_{gen} \end{bmatrix}^T$; $u_{DT} = \begin{bmatrix} \Delta T_w & \Delta T_e \end{bmatrix}^T$;

$$A_{DT} = \begin{bmatrix} 0 & 0 & 0 & 1 & 0 & 0 \\ 0 & 0 & 0 & 0 & 1 & 0 \\ 0 & 0 & 0 & 0 & 0 & 1 \\ \frac{-K_{12}}{M_1} & \frac{K_{12}}{M_1} & 0 & \frac{-(D_1+D_{12})}{M_1} & \frac{D_{12}}{M_1} & 0 \\ \frac{K_{12}}{M_2} & \frac{-(K_{12}+K_{23})}{M_2} & \frac{K_{23}}{M_2} & \frac{D_{12}}{M_2} & \frac{-(D_{12}+D_2+D_{23})}{M_2} & \frac{D_{23}}{M_2} \\ 0 & \frac{K_{23}}{M_3} & \frac{-K_{23}}{M_3} & 0 & \frac{D_{23}}{M_3} & \frac{-(D_{23}+D_3)}{M_3} \end{bmatrix};$$

$$B_{DT} = \begin{bmatrix} 0 & 0 & 0 & \frac{1}{M_1} & 0 & 0 \\ 0 & 0 & 0 & 0 & 0 & -\frac{1}{M_3} \end{bmatrix}^T; \quad C_{DT} = \begin{bmatrix} 0 & 0 & 1 & 0 & 0 & 0 \\ 0 & 0 & 0 & 0 & 0 & 1 \end{bmatrix};$$

$D_{DT} = 0_{2\times 2}$.

where, "Δ" denotes a small deviation of the variables.

2.2 DFIG model In order to model the induction generator, the stator flux orientated control strategy is adopted. Then the flux is selected as a state variable, and a 5th order dynamic model in [19] is used to describe the induction generator. The equation of motion has been included in eq.(1) and reflected in the 3rd mass. Thus, the small signal model for the induction generator is shown as follows

$$\begin{cases} \dot{X}_G = A_G X_G + B_G u_G \\ Y_G = C_G X_G + D_G u_G \end{cases} \tag{3}$$

where subscript *G* refers to DFIG, and

$X_G = \begin{bmatrix} \Delta\psi_{qs} & \Delta\psi_{ds} & \Delta\psi_{qr} & \Delta\psi_{dr} \end{bmatrix}^T$; $Y_G = \begin{bmatrix} \Delta i_{qs} & \Delta i_{ds} & \Delta T_e \end{bmatrix}^T$;

$u_G = \begin{bmatrix} \Delta u_{qs} & \Delta u_{ds} & \Delta u_{qr} & \Delta u_{dr} & \Delta\omega_r \end{bmatrix}^T$;

$$A_G = \begin{bmatrix} \frac{-\omega_b R_s X_{rr}}{D} & -\omega_s\omega_b & \frac{\omega_b R_s X_m}{D} & 0 \\ \omega_s\omega_b & \frac{\omega_b R_s X_{rr}}{D} & 0 & \frac{\omega_b R_s X_m}{D} \\ \frac{\omega_b R_r X_m}{D} & 0 & \frac{-\omega_b R_r X_{ss}}{D} & -s_0\omega_s\omega_b \\ 0 & \frac{\omega_b R_r X_m}{D} & s_0\omega_s\omega & \frac{-\omega_b R_r X_{ss}}{D} \end{bmatrix};$$

$$B_G = \begin{bmatrix} \omega_b & 0 & 0 & 0 & 0 \\ 0 & \omega_b & 0 & 0 & 0 \\ 0 & 0 & \omega_b & 0 & \omega_s\omega_b\psi_{dr0} \\ 0 & 0 & 0 & \omega_b & -\omega_s\omega_b\psi_{qr0} \end{bmatrix};$$

$$C_G = \begin{bmatrix} \frac{X_{rr}}{D} & 0 & \frac{-X_m}{D} & 0 \\ 0 & \frac{X_{rr}}{D} & 0 & \frac{-X_m}{D} \\ \frac{X_m}{D}\psi_{dr0} & \frac{-X_m}{D}\psi_{qr0} & \frac{-X_m}{D}\psi_{ds0} & \frac{X_m}{D}\psi_{qs0} \end{bmatrix};$$

$D_G = 0_{3\times 5}$; $D = X_s X_r + (X_s + X_r) X_m$; $X_{ss} = X_s + X_m$;

$X_{rr} = X_r + X_m$.

where, ψ, i and u denote flux, current and voltage of DFIG respectively, whose subscript *s* and *r* denote stator and rotor respectively, and subscript *d*, *q* denote the components in d-q frame; subscript "0" denotes the initial values of variables in steady state; R_s is the stator resistance (*p.u.*); R_r is the rotor resistance (*p.u.*); X_s is the stator reactance (*p.u.*); X_r is the rotor reactance (*p.u.*); X_m is the excitation reactance (*p.u.*); ω_s is the synchronous angular velocity; ω_b is the base angular velocity; s_0 is the slip of DFIG.

2.3 DFIG converter controller model The VSC of DFIG consists of a RSC and a GSC, which are connected back-to-back via a DC-link. Because of the variable-frequency supply provided by the DFIG converter, the rotor angular frequency and synchronous angular frequency are decoupled, which realizes the operation of a wind turbine with variable speed. The equivalent circuit of the VSC is shown in Fig.3.

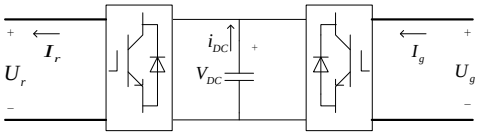

Fig.3 Equivalent circuit of the DFIG converter

2.3.1 DC-link model The power balance equation about the DFIG converter is described by

$$P_{DC} = P_r - P_g \tag{4}$$

where P_r is the rotor-side active power, P_g is the grid-side active power, and P_{DC} is the active power of the capacitor in the dc link.

Then

$$CV_{DC}\dot{V}_{DC} = u_{dg} i_{dg} + u_{qg} i_{qg} - \left(u_{dr} i_{dr} + u_{qr} i_{qr}\right) \tag{5}$$

After linearization of (5), the standard state equation of DC-link in p.u. can be obtained as follows:

$$\dot{X}_{DC} = A_{DC} X_{DC} + B_{DC} u_{DC} \tag{6}$$

where subscript *DC* refers to the DC-link, and $X_{DC} = \begin{bmatrix} \Delta V_{DC} \end{bmatrix}$;

$u_{DC} = \begin{bmatrix} \Delta u_{qg} & \Delta u_{dg} & \Delta i_{qg} & \Delta i_{dg} & \Delta u_{qr} & \Delta u_{dr} & \Delta i_{qr} & \Delta i_{dr} \end{bmatrix}^T$;

$A_{DC} = 0$; $B_{DC} = \frac{1}{CV_{DC0}} \begin{bmatrix} i_{qg0} & i_{dg0} & u_{qg0} & u_{dg0} & -i_{qr0} & -i_{dr0} & -u_{qr0} & -u_{dr0} \end{bmatrix}$.

2.3.2 RSC controller model The RSC is responsible for regulating DFIG active power and terminal voltage based on stator flux vector orientation method. The block diagram of RSC controller is shown in Fig.4, where u_{qr}^{φ} and u_{dr}^{φ} are used to control the active power and voltage of DFIG respectively. "*s*" in

the feed-forward pass of sX_m and sX_{rr} in Fig.4 represents the "slip" frequency,

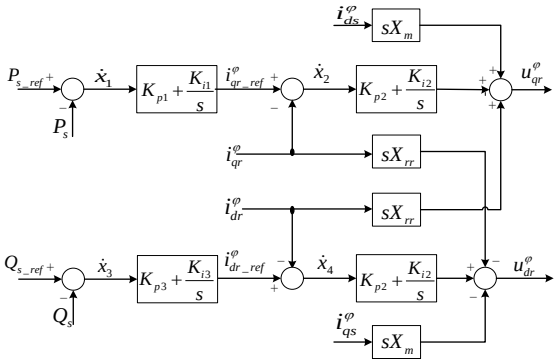

Fig.4 Block diagram of RSC controller

Assume that the converter operates fast enough so that the dynamics can be ignored and the controlled variable closely follows the given value. The corresponding equation of RSC controller is expressed as

$$\begin{cases} \dot{x}_1 = P_{s\_ref} - P_s = P_{s\_ref} - (i_{ds}^{\varphi} u_{ds}^{\varphi} + i_{qs}^{\varphi} u_{qs}^{\varphi}) \\ i_{qr\_ref}^{\varphi} = K_{p1}(P_{s\_ref} - P_s) + K_{i1} x_1 \\ \dot{x}_2 = i_{qr\_ref}^{\varphi} - i_{qr}^{\varphi} \\ \quad = K_{p1}(P_{s\_ref} - P_s) + K_{i1} x_1 - i_{qr}^{\varphi} \\ \dot{x}_3 = Q_{s\_ref} - Q_s = Q_{s\_ref} - (i_{ds}^{\varphi} u_{qs}^{\varphi} - i_{qs}^{\varphi} u_{ds}^{\varphi}) \\ i_{dr\_ref}^{\varphi} = K_{p3}(Q_{s\_ref} - Q_s) + K_{i3} x_3 \\ \dot{x}_4 = i_{dr\_ref}^{\varphi} - i_{dr}^{\varphi} \\ \quad = K_{p3}(Q_{s\_ref} - Q_s) + K_{i3} x_3 - i_{dr}^{\varphi} \\ u_{qr} = K_{p2}[K_{p1}(P_{s\_ref} - P_s) + K_{i1} x_1 - i_{qr}^{\varphi}] + K_{i2} x_2 + sX_m i_{ds}^{\varphi} + sX_{rr} i_{dr}^{\varphi} \\ u_{dr}^{\varphi} = K_{p2}[K_{p3}(Q_{s\_ref} - Q_s) + K_{i3} x_3 - i_{dr}^{\varphi}] + K_{i2} x_4 - sX_m i_{qs}^{\varphi} - sX_{rr} i_{qr}^{\varphi} \end{cases} \tag{7}$$

During linearization, we first have following equations:

$$\begin{cases} \Delta P_{s\_ref} = 0 \\ \Delta P_s = i_{ds0}^{\varphi} \Delta u_{ds}^{\varphi} + u_{ds0}^{\varphi} \Delta i_{ds}^{\varphi} + i_{qs0}^{\varphi} \Delta u_{qs}^{\varphi} + u_{qs0}^{\varphi} \Delta i_{qs}^{\varphi} \\ \Delta Q_{s\_ref} = 0 \\ \Delta Q_s = i_{ds0}^{\varphi} \Delta u_{qs}^{\varphi} + u_{qs0}^{\varphi} \Delta i_{ds}^{\varphi} - i_{qs0}^{\varphi} \Delta u_{ds}^{\varphi} - u_{ds0}^{\varphi} \Delta i_{qs}^{\varphi} \end{cases} \tag{8}$$

Then the standard state equation of RSC controller is presented as follows

$$\dot{X}_r = A_r X_r + B_r u_r \tag{9}$$

where subscript *r* denotes RSC, and

$$X_r = \begin{bmatrix} \Delta x_1 & \Delta x_2 & \Delta x_3 & \Delta x_4 \end{bmatrix}^T;$$

$$u_r = \begin{bmatrix} \Delta u_{ds}^{\phi} & \Delta u_{qs}^{\phi} & \Delta i_{ds}^{\phi} & \Delta i_{qs}^{\phi} & \Delta i_{dr}^{\phi} & \Delta i_{qr}^{\phi} & \Delta P_{s\_ref} & \Delta Q_{s\_ref} \end{bmatrix}^T;$$

$$A_r = \begin{bmatrix} 0 & 0 & 0 & 0 \\ k_{i1} & 0 & 0 & 0 \\ 0 & 0 & 0 & 0 \\ 0 & 0 & k_{i3} & 0 \end{bmatrix};$$

$$B_r = \begin{bmatrix} -i_{ds0}^{\phi} & -i_{qs0}^{\phi} & -u_{ds0}^{\phi} & -u_{qs0}^{\phi} & 0 & 0 & 1 & 0 \\ -k_{p1} i_{ds0}^{\phi} & -k_{p1} i_{qs0}^{\phi} & -k_{p1} u_{ds0}^{\phi} & -k_{p1} u_{qs0}^{\phi} & 0 & -1 & k_{p1} & 0 \\ i_{qs0}^{\phi} & -i_{ds0}^{\phi} & -u_{qs0}^{\phi} & u_{ds0}^{\phi} & 0 & 0 & 0 & 1 \\ k_{p3} i_{qs0}^{\phi} & -k_{p3} i_{ds0}^{\phi} & -k_{p3} u_{qs0}^{\phi} & k_{p3} u_{ds0}^{\phi} & -1 & 0 & 0 & k_{p3} \end{bmatrix}.$$

2.3.3 GSC Controller Model The GSC is responsible for controlling the DC-link voltage as a constant value and the output reactive power of DFIG. The block diagram of GSC controller is shown in Fig.5.

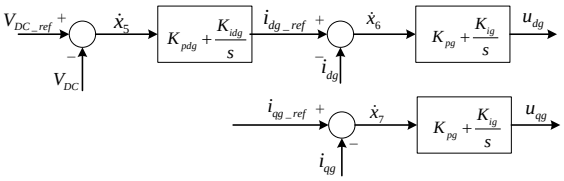

Fig.5 Block diagram of GSC controller

Similar to the RSC controller, the linearized equations of the GSC controller can be expressed as

$$\begin{cases} \Delta \dot{x}_5 = \Delta V_{DC\_ref} - \Delta V_{DC} \\ \Delta i_{dg\_ref} = K_{pdg}(\Delta V_{DC\_ref} - \Delta V_{DC}) + K_{idg} \Delta x_5 \\ \Delta \dot{x}_6 = \Delta i_{dg\_ref} - \Delta i_{dg} \\ \quad = K_{pdg}(\Delta V_{DC\_ref} - \Delta V_{DC}) + K_{idg} \Delta x_5 - \Delta i_{dg} \\ \Delta \dot{x}_7 = \Delta i_{qg\_ref} - \Delta i_{qg} \\ \Delta u_{dg} = K_{pg}[K_{pdg}(\Delta V_{DC\_ref} - \Delta V_{DC}) + K_{idg} \Delta x_5 - \Delta i_{dg}] + K_{ig} \Delta x_6 \\ \Delta u_{qg} = K_{pg}(\Delta i_{qg\_ref} - \Delta i_{qg}) + K_{ig} \Delta x_7 \end{cases} \tag{10}$$

where, $\Delta V_{DC\_ref} = 0$ and $\Delta i_{qg\_ref} = 0$.

The standard state equation of GSC controller is

$$\dot{X}_g = A_g X_g + B_g u_g \tag{11}$$

where subscript *g* refers to GSC, and

$$X_g = \begin{bmatrix} \Delta x_5 & \Delta x_6 & \Delta x_7 \end{bmatrix}^T;$$

$$u_g = \begin{bmatrix} \Delta V_{DC\_ref} & \Delta V_{DC} & \Delta i_{qg\_ref} & \Delta i_{dg} & \Delta i_{qg} \end{bmatrix}^T;$$

$$A_g = \begin{bmatrix} 0 & 0 & 0 \\ k_{idg} & 0 & 0 \\ 0 & 0 & 0 \end{bmatrix}; B_g = \begin{bmatrix} 1 & -1 & 0 & 0 & 0 \\ k_{pdg} & -k_{pdg} & 0 & -1 & 0 \\ 0 & 0 & 1 & 0 & -1 \end{bmatrix}.$$

2.4 Transmission line model In an actual wind power system, a series compensation capacitor is usually integrated in the transmission line to enhance the transmission capacity. On the other hand, the series compensation capacitor will influence both the shaft torsional vibration frequency and damping, and even causes SSR problem. So a series compensation capacitor is included in the transmission line in this research. Then the transmission line is equivalent to a RLC line model to study the shaft torsional vibration characteristics to reflect actual situations and capture the generality. Selecting the current and the voltage of the series compensation capacitor as the state variables, the standard state equation of the transmission line in xy-frame is expressed as

$$\begin{cases} \dot{X}_{TL} = A_{TL} X_{TL} + B_{TL} u_{TL} \\ Y_{TL} = C_{TL} X_{TL} + D_{TL} u_{TL} \end{cases} \tag{12}$$

where subscript *TL* refers to the transmission line, and

$$X_{TL} = \begin{bmatrix} \Delta i_x & \Delta i_y & \Delta u_{cx} & \Delta u_{cy} \end{bmatrix}^T;$$

$$u_{TL} = \begin{bmatrix} \Delta u_{x1} & \Delta u_{y1} & \Delta u_{x2} & \Delta u_{y2} \end{bmatrix}^T;$$

$$A_{TL}=\begin{bmatrix} -\omega_b r/x & \omega_b & -\omega_b/x & 0 \\ -\omega_b & -\omega_b r/x & 0 & -\omega_b/x \\ -\omega_b/x & 0 & 0 & \omega_b \\ 0 & -\omega_b/x & -\omega_b & 0 \end{bmatrix};$$

$$B_{TL}=\begin{bmatrix} \omega_b/x & 0 & -\omega_b/x & 0 \\ 0 & \omega_b/x & 0 & -\omega_b/x \\ 0 & 0 & 0 & 0 \\ 0 & 0 & 0 & 0 \end{bmatrix};\ C_{TL}=\begin{bmatrix} 1 & 0 & 0 & 0 \\ 0 & 1 & 0 & 0 \end{bmatrix};$$

$D_{TL}=0_{2\times 4}$. where ω_b is the base angular frequency of the system, 2π×50; r and x are the resistance and reactance of the transmission line respectively.

After considering the resistance of the inductor, the filter is equivalent to a RL line model. Similar to the transmission line, the state space equation of the filter can be expressed as

$$\begin{cases} \dot{X}_{RL}=A_{RL}X_{RL}+B_{RL}u_{RL} \\ Y_{RL}=C_{RL}X_{RL}+D_{RL}u_{RL} \end{cases} \tag{13}$$

where subscript *RL* represents the filter and

$$X_{RL}=Y_{RL}=\begin{bmatrix}\Delta i_x & \Delta i_y\end{bmatrix}^T;\ u_{RL}=\begin{bmatrix}\Delta u_x & \Delta u_y\end{bmatrix}^T;$$

$$A_{RL}=\begin{bmatrix} -\omega_b r_L/x_L & \omega_b \\ -\omega_b & -\omega_b r_L/x_L \end{bmatrix};\ B_{RL}=\begin{bmatrix} \omega_b/x_L & 0 \\ 0 & \omega_b/x_L \end{bmatrix};$$

$$C_{RL}=\begin{bmatrix} 1 & 0 \\ 0 & 1 \end{bmatrix};\ D_{RL}=0.$$

where r_L and x_L are the resistance and reactance of the filter respectively.

Similarly, the compensation capacitor can be modeled as

$$\begin{cases} \dot{X}_C=A_C X_C+B_C u_C \\ Y_C=C_C X_C+D_C u_C \end{cases} \tag{14}$$

where, subscript *C* represents the compensation capacitor and

$$X_C=Y_C=\begin{bmatrix}\Delta u_{Cx} & \Delta u_{Cy}\end{bmatrix}^T;\ u_C=\begin{bmatrix}\Delta i_{Cx} & \Delta i_{Cy}\end{bmatrix}^T;$$

$$A_C=\begin{bmatrix} 0 & \omega_b \\ -\omega_b & 0 \end{bmatrix};\ B_C=\begin{bmatrix} -\omega_b x_C & 0 \\ 0 & -\omega_b x_C \end{bmatrix};\ C_C=\begin{bmatrix} 1 & 0 \\ 0 & 1 \end{bmatrix};$$

$D_C=\text{zeros}(2,2)$.

where x_C is the reactance of the capacitor.

2.5 Unified small signal model of DFIG Based on the small signal model developed for each component above, the unified small signal model of the grid-connected DFIG-based wind power system can be established. The interaction between different modules is shown in Fig.6.

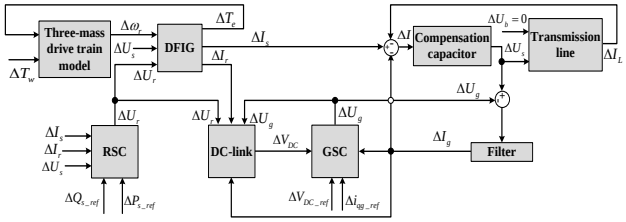

Fig.6 Schematic diagram of the small-signal model

By grouping the equations (2), (3), (6), (9), (11), (12), (13) and (14) together, the unified small signal model can be expressed as follows

$$\begin{cases} \dot{X}_{DFIG}=A_{DFIG}X_{DFIG}+B_{DFIG}u_{DFIG} \\ Y_{DFIG}=C_{DFIG}X_{DFIG}+D_{DFIG}u_{DFIG} \end{cases} \tag{15}$$

where $X_{DFIG}=\begin{bmatrix}X_{DT} & X_G & X_r & X_{DC} & X_g & X_C & X_{RL} & X_{TL}\end{bmatrix}^T$;

$$A_{DFIG}=\begin{bmatrix} \boldsymbol{A}_{DT} & \boldsymbol{A}_{G\_DT} & & & & & & \\ \boldsymbol{A}_{DT\_G} & \boldsymbol{A}_{G} & \boldsymbol{A}_{r\_G} & & & & & \\ & \boldsymbol{A}_{G\_r} & \boldsymbol{A}_{r} & \boldsymbol{A}_{DC\_r} & & & & \\ & & \boldsymbol{A}_{r\_DC} & \boldsymbol{A}_{DC} & \boldsymbol{A}_{g\_DC} & & & \\ & & & \boldsymbol{A}_{DC\_g} & \boldsymbol{A}_{g} & \boldsymbol{A}_{C\_g} & & \\ & & & & \boldsymbol{A}_{g\_C} & \boldsymbol{A}_{C} & \boldsymbol{A}_{RL\_C} & \\ & & & & & \boldsymbol{A}_{C\_RL} & \boldsymbol{A}_{RL} & \boldsymbol{A}_{TL\_RL} \\ & & & & & & \boldsymbol{A}_{RL\_TL} & \boldsymbol{A}_{TL} \end{bmatrix};$$

$$B_{DFIG}=\begin{bmatrix} 0 & 0 & 0 & \dfrac{1}{M_1} & 0 & 0 & \mathbf{0}_{1\times 20} \end{bmatrix}^T;\quad C_{DFIG}=\begin{bmatrix}\mathbf{0}_{2\times 24} & \mathbf{I}_{2\times 2}\end{bmatrix};$$

$D=\mathbf{0}$. where $\boldsymbol{A}_{DT\_G}$ ($\boldsymbol{A}_{G\_DT}$), $\boldsymbol{A}_{G\_r}$ ($\boldsymbol{A}_{r\_G}$), $\boldsymbol{A}_{r\_DC}$ ($\boldsymbol{A}_{DC\_r}$), $\boldsymbol{A}_{DC\_g}$ ($\boldsymbol{A}_{g\_DC}$), $\boldsymbol{A}_{g\_C}$ ($\boldsymbol{A}_{C\_g}$), $\boldsymbol{A}_{C\_RL}$ ($\boldsymbol{A}_{RL\_C}$), $\boldsymbol{A}_{RL\_TL}$ ($\boldsymbol{A}_{TL\_RL}$) represent the correlations between adjacent models.

3. Model of a DFIG-based wind farm

To analyze the torsional vibration characteristics of the WF, a WF with several identical 2MW, 690V DFIG-based wind turbines is designed. The schematic diagram of the WF is shown in Fig.7. Assume that the blade diameter of each WTG is 40m, the lateral distance between every two WTGs is set as 100m, and the vertical distance is also set as 100m. Every WTG is connected to the 10kV bus via a transformer and the transmission line.

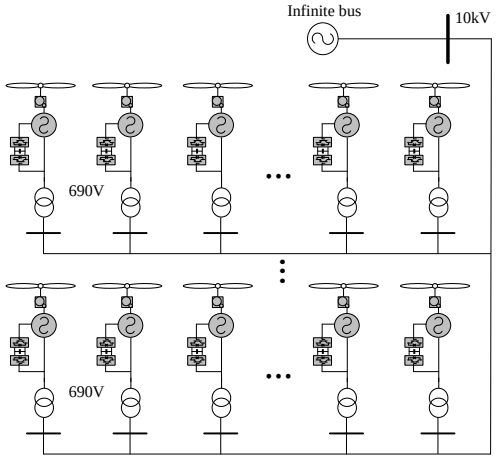

Fig.7 Schematic diagram of the DFIG-based WF

Based on the small signal model of a single DFIG-based wind turbine developed in Fig.6, the small signal model for the DFIG-based WF is built in MATLAB/SIMULINK with each component jointed together, which is easy to realize. The parameters of the DFIG-based wind turbine are listed in the Appendix.

It is noted that the state matrix A in equation (15) is a 26 order

square matrix. If the WF in Fig.7 is analyzed directly with the application of equation (15), then the state matrix of the WF, e.g. including 6 DFIGs, will be a 150 order matrix, which is rather complex to solve. Also as the number of WTGs increases, the perplexity of the mathematical model and its computation complexity will increase significantly, and the time domain simulation for the WF is rather difficult even impossible to conduct. Therefore, a reduced order equivalent model of the WF is necessary for further deep research.

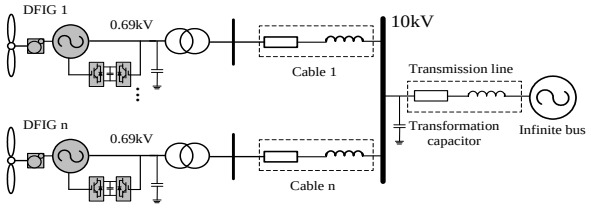

Fig.8 Schematic diagram of multi-WTG system

Take the multi-DFIGs system shown in Fig.8 as an example. Each WTG is connected to the 10kV bus with a cable first and then the 10kV bus of the WF is connected to the infinite bus with a long transmission line.

The schematic diagram of the small signal model for the WF is shown in Fig.9. The transformer together with the cable is equivalent to a RLC line model and the state space equation is the same with that shown in equation (12). The transformation capacitor is actually the capacitor of the transmission line and the output current of the DFIGs is converted into the input voltage of the transformer & cable, thus the capacitor is also called transformation capacitor, whose state space equation is the same with equation (14).

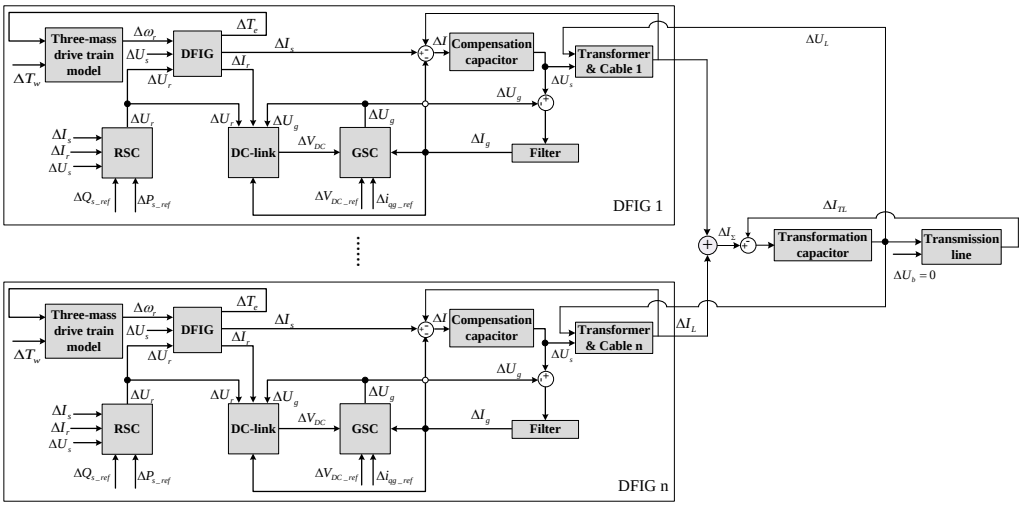

Fig.9 schematic diagram for the small signal model of the WF

According to equation (15), the state space equation of the multi-DFIGs system in Fig.9 can be expressed as follows

$$\begin{bmatrix} \dot{X}_{DFIG1} \\ \vdots \\ \dot{X}_{DFIGn} \\ \dot{X}_{TC} \\ \dot{X}_{TL} \end{bmatrix} = \begin{bmatrix} A_{DFIG1} & & & A_{DFIG1\_TC(V)} & \\ & \ddots & & \vdots & \\ & & A_{DFIGn} & A_{DFIGn\_TC(V)} & \\ & & & A_{TC} & \\ & & & & A_{TL} \end{bmatrix} \cdot \begin{bmatrix} X_{DFIG1} \\ \vdots \\ X_{DFIGn} \\ X_{TC} \\ X_{TL} \end{bmatrix} + \begin{bmatrix} B_{DFIG1} & & & & \\ & \ddots & & & \\ & & B_{DFIGn} & & \\ & & & B_{TC} & \\ & & & & B_{TL} \end{bmatrix} \cdot \begin{bmatrix} u_{DFIG1} \\ \vdots \\ u_{DFIGn} \\ u_{TC} \\ u_{TL} \end{bmatrix} \tag{16}$$

where $X_{DFIGi} = \begin{bmatrix} X_{DTi} & X_{Gi} & X_{ri} & X_{DCi} & X_{gi} & X_{Ci} & X_{RLi} & X_{Cablei} \end{bmatrix}^T$

$, i = 1, 2, \cdots, n$; subscript *TC* denotes the transformation capacitor; subscript *RL* denotes the filter; subscript *Cable* denotes the equivalent RL line model of the transformer & cable; subscript *TL* denotes the transmission line.

As for the transformation capacitor, its input and output satisfy

$$\begin{cases} u_{TC} = \sum_{i=1}^{n} Y_{DFIGi} = \begin{bmatrix} C_{DFIG1} & & \\ & \ddots & \\ & & C_{DFIGn} \end{bmatrix} \cdot \begin{bmatrix} X_{DFIG1} \\ \vdots \\ X_{DFIGn} \end{bmatrix} \\ Y_{TC} = u_{Cable1} = \cdots = u_{Cablen} = C_{TC} X_{TC} \end{cases} \tag{17}$$

where, u_{TC} and Y_{TC} are the input current and output voltage of the transformation capacitor, respectively; u_{Cablei} is the input voltage of the transformer & cable model.

By substituting equation (17) into (16), the following equation can be derived

$$\begin{bmatrix} \dot{X}_{DFIG1} \\ \vdots \\ \dot{X}_{DFIGn} \\ \dot{X}_{TC} \\ \dot{X}_{TL} \end{bmatrix} = \begin{bmatrix} A_{DFIG1} & & & A_{DFIG1\_TC(V)} & \\ & \ddots & & \vdots & \\ & & A_{DFIGn} & A_{DFIGn\_TC(V)} & \\ & & & A_{TC} & \\ & & & & A_{TL} \end{bmatrix} \cdot \begin{bmatrix} X_{DFIG1} \\ \vdots \\ X_{DFIGn} \\ X_{TC} \\ X_{TL} \end{bmatrix} + \begin{bmatrix} B_{DFIG1} & & & & \\ & \ddots & & & \\ & & B_{DFIGn} & & \\ & & & B_{TC} & \\ & & & & B_{TL} \end{bmatrix} \cdot \begin{bmatrix} u_{DFIG1} \\ \vdots \\ u_{DFIGn} \\ \sum_{i=1}^{n} C_{DFIGi} \cdot X_{DFIGi} \\ u_{TL} \end{bmatrix} \tag{18}$$

Equation (18) can be further expressed as

$$\begin{bmatrix} \dot{X}_{DFIG1} \\ \vdots \\ \dot{X}_{DFIGn} \\ \dot{X}_{TC} \\ \dot{X}_{TL} \end{bmatrix} = \begin{bmatrix} A_{DFIG1} & & & A_{DFIG1\_TC(V)} & \\ & \ddots & & \vdots & \\ & & A_{DFIGn} & A_{DFIGn\_TC(V)} & \\ B_{TC}C_{DFIG1} & \cdots & B_{TC}C_{DFIGn} & A_{TC} & \\ & & & & A_{TL} \end{bmatrix} \cdot \begin{bmatrix} X_{DFIG1} \\ \vdots \\ X_{DFIGn} \\ X_{TC} \\ X_{TL} \end{bmatrix} + \begin{bmatrix} B_{DFIG1} & & & \\ & \ddots & & \\ & & B_{DFIGn} & \\ & & & B_{TL} \end{bmatrix} \cdot \begin{bmatrix} u_{DFIG1} \\ \vdots \\ u_{DFIGn} \\ u_{TL} \end{bmatrix} \quad (19)$$

In order to conduct eigenvalue analysis conveniently, the state space matrix of equation (19) is denoted by

$$A_{sys} = \begin{bmatrix} A_{DFIG1} & \mathbf{0} & \mathbf{0} & A_{DFIG1\_TC(V)} & \mathbf{0} \\ \mathbf{0} & \ddots & \mathbf{0} & \vdots & \vdots \\ \mathbf{0} & \mathbf{0} & A_{DFIGn} & A_{DFIGn\_TC(V)} & \mathbf{0} \\ B_{TC}C_{DFIG1} & \cdots & B_{TC}C_{DFIGn} & A_{TC} & \mathbf{0} \\ \mathbf{0} & \cdots & \mathbf{0} & \mathbf{0} & A_{TL} \end{bmatrix} = \begin{bmatrix} A_{DFIG} & \mathbf{0} & \mathbf{0} & M_{DFIGV} \\ \mathbf{0} & \ddots & \mathbf{0} & \vdots \\ \mathbf{0} & \mathbf{0} & A_{DFIG} & M_{DFIGV} \\ M_{DFIGI} & \cdots & M_{DFIGI} & A_{RLC} \end{bmatrix} \quad (20)$$

Because all the DFIGs in Fig.7 are in completely symmetry connection, $A_{DFIGi}(i=1,2,\cdots n)$ in (20) are all the same and denoted by A_{DFIG}. Similarly, $M_{DFIGV} = \begin{bmatrix} A_{DFIGi\_TC(V)} & \mathbf{0} \end{bmatrix}$ i=1, 2, …, n; $M_{DFIGI} = \begin{bmatrix} B_{TC}C_{DFIGi} \\ \mathbf{0} \end{bmatrix} (i=1,2,\cdots n)$; $A_{RLC} = \begin{bmatrix} A_{TC} & \mathbf{0} \\ \mathbf{0} & A_{TL} \end{bmatrix}$.

Based on matrix theory, A_{sys} can be converted into an orthogonal one by using matrix transformation, represented by A'_{sys} [20].

$$A'_{sys} = P^{-1}A_{sys}P = \begin{bmatrix} A_{DFIG} & & & \\ & \ddots & & \\ & & A_{DFIG} & M_{DFIGV} \\ & & NM_{DFIGI} & A_{RLC} \end{bmatrix} \quad (21)$$

where, $P = \begin{bmatrix} k_{11}I & \cdots & k_{1(N-1)}I & I \\ k_{21}I & \cdots & k_{2(N-1)}I & I \\ \vdots & \ddots & \vdots & \vdots \\ k_{N1}I & \cdots & k_{N(N-1)}I & I \\ & & & I \end{bmatrix}$ and the coefficients must satisfy $\sum_{i=1}^{N} k_{ij} = 0,\ j = 1,2,\cdots,N-1$.

For any two similar matrices, their eigenvalues are the same. Thus the eigenvalues of A_{sys} can be obtained through calculating those of A'_{sys}, which is achieved as follows.

$$\begin{aligned} \lambda(A'_{sys}) &= \left\{ \underbrace{\lambda(A_{DFIG})\ \lambda(A_{DFIG})\ \cdots\ \lambda(A_{DFIG})}_{N-1}\ \lambda\begin{Bmatrix} A_{DFIG} & M_{DFIGV} \\ NM_{DFIGI} & A_{RLC} \end{Bmatrix} \right\} \\ &= \left\{ \underbrace{\lambda(A_{DFIG})\ \lambda(A_{DFIG})\ \cdots\ \lambda(A_{DFIG})}_{N-1}\ \lambda\begin{Bmatrix} A_{DFIG} & A_{DFIG\_TC(V)} & 0 \\ NB_{TC}\cdot C_{DFIG} & A_{TC} & 0 \\ 0 & 0 & A_{TL} \end{Bmatrix} \right\} \end{aligned} \quad (22)$$

From equation (22), it is found that the eigenvalues of A_{sys} are derived from two parts: N-1 identical matrices A_{DFIG} and one modified matrix. Namely, the multi-DFIGs system in Fig.8 can be simplified as a system consisting of n single-DFIGs. The n-1 identical single-DFIGs are connected to the infinite bus directly, while the n*th* DFIG with modified output current is connected to the infinite bus via a transmission network. The output current of the modified DFIG is n times that of the original single DFIG.

The equivalent model of the WF is shown in Fig.10. Therefore for the multi-DFIGs system, there will be n-1 groups of identical eigenvalues. As a result, the shaft torsional vibration analysis for the WF is simplified significantly.

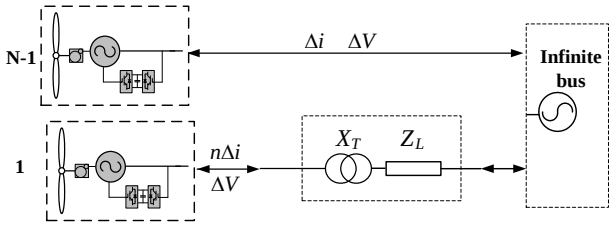

Fig.10 Equivalent model of the multi-DFIGs WF

Table I. Eigenvalues of the WF (imaginary part represents oscillation frequency)

Number of DFIG	1	2	3	4	5	6
Oscillation modes of the low-speed shaft	-0.154± 14.6525i	-0.1545±14.6525i -0.1533±14.5764i	-0.1545±14.6525i -0.1533±14.5764i -0.1533±14.5764i	-0.1545±14.6525i -0.1533±14.5764i -0.1533±14.5764i -0.1533±14.5764i	-0.1545±14.6525i -0.1533±14.5764i -0.1533±14.5764i -0.1533±14.5764i -0.1533±14.5764i	-0.1545±14.6525i -0.1533±14.5764i -0.1533±14.5764i -0.1533±14.5764i -0.1533±14.5764i -0.1533±14.5764i
Oscillation modes of the high-speed shaft	-0.4072±2.884i	-0.0161±2.8194i -0.5416± 2.8834i	-0.0197±2.8198i -0.5416± 2.8834i -0.5416± 2.8834i	-0.0214±2.8199i -0.5416± 2.8834i -0.5416± 2.8834i -0.5416± 2.8834i	-0.0224±2.8201i -0.5416± 2.8834i -0.5416± 2.8834i -0.5416± 2.8834i -0.5416± 2.8834i	-0.023± 2.8201i -0.5416± 2.8834i -0.5416± 2.8834i -0.5416± 2.8834i -0.5416± 2.8834i -0.5416± 2.8834i

When some wind turbines' operating conditions are different from others, the proposed method can also work well after extending the model a little. Supposing that the first DFIG of a wind farm runs at 25% of rated power. The remaining n-1 DFIGs all run at rated power. The state space matrix of the wind farm system consisting of n wind turbines is denoted by

$$A_{sys} = \begin{bmatrix} A'_{DFIG} & \mathbf{0} & \mathbf{0} & \mathbf{0} & M'_{DFIGV} \\ \mathbf{0} & \ddots & \mathbf{0} & \mathbf{0} & \vdots \\ \mathbf{0} & \mathbf{0} & A_{DFIG} & \mathbf{0} & M_{DFIGV} \\ \mathbf{0} & \mathbf{0} & \mathbf{0} & A_{DFIG} & M_{DFIGV} \\ M'_{DFIGI} & \cdots & M_{DFIGI} & M_{DFIGI} & A_{RLC} \end{bmatrix}$$

We can also simplify eigenvalue calculation of A_{sys} based on matrix transformation and the characteristic of arrowhead matrix.

$$\left|\lambda I - A_{sys}\right| = \left|\lambda I - A'_{DFIG}\right| \bullet \left|\lambda I - A_{DFIG}\right|^{m-1} \bullet \left|\lambda I - A_{RLC} - M'_{DFIGI}\left(\lambda I - A'_{DFIG}\right)^{-1} M'_{DFIGV} - (n-1) M_{DFIGI}\left(\lambda I - A_{DFIG}\right)^{-1} M_{DFIGV}\right|$$

4. Studied cases

4.1 Torsional vibration analysis with the small signal model of the WF

4.1.1 Modal analysis To study the shaft torsional vibration characteristic of the DFIG-based WF, the small signal model of Fig.7 is established in MATLAB/SIMULINK first. Varying the number of DFIG from 1 to 6, the shaft torsional vibration characteristics of the low-speed and high-speed shaft can be obtained through the sensitivity analysis, as shown in Table I. The modes of the low-speed and high-speed shafts are separated according to the participation factors, which are used to measure the relative participation of system variables in the oscillation modes [19].

In Table I, all the oscillation modes are obtained when the DFIGs are operated at their nominal states. It should also be noted that the eigenvalues are calculated when the damping of the shaft system is zero. The imaginary part has been converted into the corresponding oscillation frequency through divided by 2π. It can be seen from Table I that for a WF with n DFIGs, only two kinds of oscillation modes appear in the torque of the low-speed shaft. One oscillation frequency is 14.6525Hz, which is the same with that of the single DFIG, and the absolute value of the real part is a little larger than that of the single DFIG, which means the damping of this mode increases. The other n-1 repeated oscillation frequencies are 14.5764Hz, which is lower than that of the single DFIG, and the absolute value of the real parts is a little smaller than that of the single DFIG, which means the damping of these modes decreases. So, in a WF, the natural oscillation frequency of the low-speed shaft differs from that of the one DFIG case. Also, the shaft torsional vibration for some DFIGs is easier to be excited for the decreased damping.

Similarly, there exist two oscillation modes in the torque of the high-speed shaft as well. The n-1 repeated oscillation frequencies are 2.8834Hz, which is lower than that of the single DFIG, and the absolute value of the real parts is larger than that of the single DFIG, which means the damping of these modes increase. The other oscillation frequency of the high-speed shaft decreases from 2.8194Hz to 2.8201Hz with the number of DFIGs increasing, and the damping decreases first and then began to increase. While the absolute value of the damping is much smaller than the single DFIG, which means the corresponding mode is much easier to be excited in the transient process. The phenomenon means that in a multi-DFIGs WF, the shaft torsional vibration of the high-speed shaft for one DFIG is quite easy to be excited and effective damping strategy is necessary. On the other hand, a WF with more DFIGs can help damping the shaft torsional vibration.

4.1.2 Time domain simulation A WF made up of three DFIGs is taken as an example to demonstrate the results obtained from modal analysis. The time domain simulation is conducted in MATLAB/SIMULINK and the parameters are the same with that of the small signal model except for the damping of the shaft system. After the WF is operated in its stable state, a 1% voltage sag is imposed on the power system at t=1s, which sustains for a period of 0.1s. In order to achieve converged shaft torque in a short time, the damping of the shaft system of the time-domain model is set at a relatively high value. Simulation results are illustrated in Fig.11.

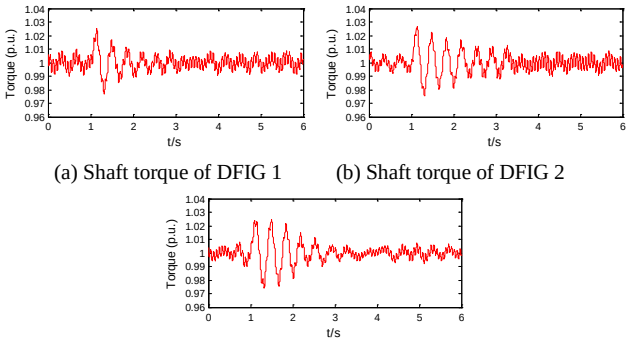

(a) Shaft torque of DFIG 1 (b) Shaft torque of DFIG 2

(c) Shaft torque of DFIG 3

Fig.11 Torsional vibration of a three-DFIG WF

It can be observed from Fig.11 that the shaft torsional vibration is excited at 1s by the small electrical disturbance. The oscillation calms down gradually because of the positive damping. Though the shaft torque of the three DFIGs are in oscillation, they are all around 1 p.u.. After the small electrical disturbance appears at 1s, the maximum shaft torque of three DFIGs reaches 1.028 p.u., 1.03 p.u. and 1.024 p.u. respectively. At t=1.1s, after the voltage sag is removed, the torsional vibration of the shaft begin to decay, which can be explained using the results in Table I. The real part of the oscillation modes of the 3 DFIGs in Table I is negative, which means the damping for the mode is positive and the shaft torsional vibration will decay after the disturbance is removed.

The frequency spectrum of the shaft torques in Fig.11 is shown in Fig.12. It can be seen that the shaft torques oscillate at six frequencies. The frequencies of 2.766Hz, 2.67Hz and 2.67Hz are for the oscillation modes of the low-speed shaft for the three wind turbines, and that of 14.69Hz, 14.59Hz and 14.59Hz are for the oscillation modes of the high-speed shaft. Two kinds of torsional modes appear in the high and low shaft torque respectively, which are consistent with the results derived from the modal analysis.

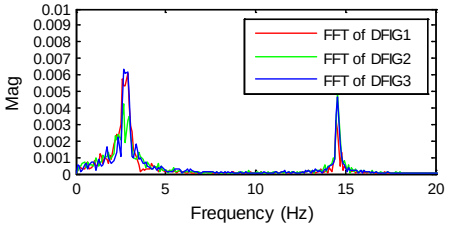

Fig.12 Frequency spectrum of the three-DFIGs WF

4.2 Torsional vibration analysis with the equivalent model of the WF

To verify the proposed equivalent model for a WF, the equivalent model of a WF composed of 6 DFIGs is established. As has been discussed above, the six-DFIGs WF can be simplified into 6 single-DFIG systems. 5 single-DFIGs are connected to the infinite bus directly, and the other one modified DFIG connected to the infinite bus via a transmission network, including a transformer and a transmission line. Then the small signal model of the equivalent multi-DFIGs system is built in MATLAB/SIMULINK with each component jointed together. The parameters for DFIGs are shown in the Appendix. Torsional vibration modes of the low speed and the high-speed shafts can be obtained by sensitivity analysis, as shown in Table II.

Table II. Torsional vibration modes of the 6-DFIGs WF

	Eigenvalue	Frequency/Hz
5 single-DFIGs	-0.1533±14.5764i	14.5764
	-0.5416± 2.8834i	2.8834
1 modified DFIG	-0.1545±14.6525i	14.6525
	-0.0223± 2.8211i	2.8211

As shown in Table II, there are four kinds of torsional modes in the equivalent model. There exist one frequency of 14.6525Hz and 5 repeated frequencies of 14.5764Hz in the low-speed shaft torque. There exist one frequency of 2.8211Hz and 5 repeated frequencies of 2.8834Hz in the high-speed shaft torque. Both the oscillation frequency and the damping are for the 5 single DFIGs are the same with that shown in Table I. As for the modified DFIG, the oscillation frequency and the damping for the low-speed shaft is the same with that in Table I. While the oscillation frequency for the high-speed shaft is 2.8211 Hz, a litter higher than 2.8201 Hz in Table I. At the same time, the damping is 0.0223, a little smaller than 0.023 shown in Table I. Thus, the equivalent model maintains the torsional vibration modes of the original small-signal model completely.

Torsional vibration modes of the low speed and the high-speed shafts of the (1+5)-DFIGs wind farm are obtained by the original model and the equivalent model respectively, as shown in Table III. The first DFIG runs at 25% of rated power. The remaining 5 DFIGs run at rated power. According to the results in Table III, the equivalent model can also maintain the torsional vibration modes of the original small-signal model when DFIGs have different operating conditions.

Table III. Torsional vibration modes of the (1+5)-DFIGs WF

Adopted model		Eigenvalue	Frequency/Hz
Original model	DFIG1	-0.1185±14.5793i	14.5793
		-0.2724±2.9667i	2.9667
	DFIG2	-0.1533±14.5764i	14.5764
		-0.5416±2.8834i	2.8834
	DFIG3	-0.1533±14.5764i	14.5764
		-0.5416±2.8834i	2.8834
	DFIG4	-0.1533±14.5764i	14.5764
		-0.5416±2.8834i	2.8834
	DFIG5	-0.1533±14.5764i	14.5764
		-0.5416±2.8834i	2.8834
	DFIG6	-0.1547±14.6525i	14.6525
		-0.0226±2.8198i	2.8198
Equivalent model	1 single-DFIG (25% power)	-0.1185±14.5793i	14.5793
		-0.2724±2.9667i	2.9667
	4 single-DFIGs (100% power)	-0.1533±14.5764i	14.5764
		-0.5416±2.8834i	2.8834
	1 modified DFIG	-0.1547±14.6525i	14.6525
		-0.0223±2.8205i	2.8205

The equivalent modeling method proposed in this paper brings a significant reduction in the system order by using matrix transformation and the problem of "curse of dimensionality" appearing in modeling for large-scale WFs can be avoided.

5. Conclusions

Through developing small signal model for DFIG-based wind turbines first, that for a multi-DFIGs WF is established. At the same time, an equivalent model for the WF is proposed. Through conducting simulation in MATLAB/SIMULINK, the effectiveness of the proposed equivalent model is validated and the conclusions are drawn then summarized as follows.

- For a DFIG-based WF with N identical WTGs, there are two kinds of torsional modes in the high speed and low-speed shaft torque respectively. For the low-speed shaft, there exist one single oscillation frequency, which is the same with that of the single DFIG case, and N-1 repeated oscillation frequencies. For the high-speed shaft, there exist one single oscillation frequency, which decreases first and then increases with the number of DFIGs increasing, and N-1 repeated oscillation frequencies.
- With the number of DFIGs in a WF increasing, the complexity of the mathematical model and its computation will increase significantly. The proposed equivalent model of the WF is able to simplify the original small signal model a lot. By an appropriate similarity transformation, the N-DFIGs WF can be equivalent to N-1 identical single DFIGs, which have the same eigenvalues, and one N-time-current modified DFIG. Therefore only two torsional frequencies need to be analyzed in the equivalent model, which will reduce the model complexity and improve the computation speed.

Acknowledgement

This work is financially supported by the National Natural Science Foundation of China (51277119).

Appendix

All the parameters in this paper are in their p.u. value and the base power is 2 MW.

Induction generator: n_p=2; X_m=3.9507p.u.; X_s=0.0924p.u.; X_r=0.0990 p.u.; Rs=0.0046p.u.; Rr=0.0055 p.u..

Transmission line: X_T=0.044 p.u.; R_T=0.007 p.u.; X_L=8.402 p.u.; R_L=0.8402 p.u.; X_B=0.060 p.u.; R_B=0 p.u.; X_{pc}=2 p.u.. Here, R_T and X_T represent the resistance and reactance of the transformer; R_L and X_L represent the resistance and reactance of the transmission line; R_B and X_B represent the resistance and reactance of the infinite bus system; X_{pc} represents the reactance of the compensation capacitor.

DFIG converter: C_{DC}=2.591p.u.; X_{con}=0.0024p.u.; R_{con}=0.0024p.u.; K_{p1}=0.02; K_{i1}=0.01; K_{p2}=0.02; K_{i2}=0.01; K_{p3}=0.02; K_{i3}=0.01; K_{pdg}=18; K_{idg}=1; K_{pg}=50; K_{ig}=1. Here, C_{DC} is the capacitor value of the DC-link; R_{con} and X_{con} are the resistance and reactance of the converter.

References

(1) Li, S. Y., Sun, Y., Wu, T., Li, Q. J., & Liu, H. Analysis of Small Signal Stability of Grid-Connected Doubly Fed Induction Generators. In *Power and Energy Engineering Conference (APPEEC), 2010 Asia-Pacific* (pp. 1-4). IEEE.

(2) Ahmed, H. Reactive power and voltage control in grid-connected wind farms: an online optimization based fast model predictive control approach. *Electrical Engineering* 2015; 97(1), 35-44.

(3) Gautam, D., Vittal, V., & Harbour, T. Impact of increased penetration of DFIG-based wind turbine generators on transient and small signal stability of power systems. *IEEE Transactions on Power Systems* 2009; 24(3), 1426-1434.

(4) Badrzadeh, B., & Salman, S. K. Investigation of the torsional vibration and transient stability margin for doubly-fed induction generators. In *Sustainable Alternative Energy (SAE), 2009 IEEE PES/IAS Conference on* (pp. 1-8). IEEE.

(5) Xu, L., & Wang, Y. Dynamic modeling and control of DFIG-based wind turbines under unbalanced network conditions. *IEEE Transactions on Power Systems* 2007; 22(1), 314-323.

(6) Bejaoui, M., Slama-Belkhodja, I., Monmasson, E., Marinescu, B., &

Charaabi, L. FPGA design of a robust phase locked loop algorithm for a three phase PWM grid connected converter. In *2009 13th European Conference on Power Electronics and Applications*.
(7) Altun, H., & Sünter, S. Modeling, simulation and control of wind turbine driven doubly-fed induction generator with matrix converter on the rotor side. *Electrical Engineering* 2013; 95(2), 157-170.
(8) Kayikçi, M., & Milanović, J. V. Assessing transient response of DFIG-based wind plants—The influence of model simplifications and parameters. *IEEE Transactions on Power Systems* 2008; 23(2), 545-554.
(9) Mei, F., & Pal, B. C. Modelling and small-signal analysis of a grid connected doubly-fed induction generator. *Power Engineering Society General Meeting* 2005; 2101-2108.
(10) Fan, Lingling, et al. Modal analysis of a DFIG-based WF interfaced with a series compensated network. IEEE Transactions on Energy Conversion 2011; 26.4: 1010-1020.
(11) Santoso, S., & Le, H. T. Fundamental time–domain wind turbine models for wind power studies. *Renewable Energy* 2007; 32(14), 2436-2452.
(12) Muyeen, S. M., Ali, M. H., Takahashi, R., Murata, T., Tamura, J., Tomaki, Y., & Sasano, E. Transient stability analysis of wind generator system with the consideration of multi-mass shaft model. *IEEE International Conference on Power Electronics and Drives Systems, 2005. PEDS 2005*. (Vol. 1, pp. 511-516).
(13) Lei, Ting, Mike Barnes, and Meliksah Ozakturk. Doubly-fed induction generator wind turbine modelling for detailed electromagnetic system studies. *IET Renewable Power Generation* 2013; 7.2: 180-189.
(14) He, Jianming, Lin Guan, and Xinming Fan. Equivalent Models of Wind Farms with Fixed Speed Wind Turbines. *Unifying Electrical Engineering and Electronics Engineering*. Springer New York, 2014. 1055-1063.
(15) Tabesh, Ahmadreza, and Reza Iravani. Small-signal dynamic model and analysis of a fixed-speed WF-a frequency response approach. IEEE Transactions on Power Delivery 2006; 21.2: 778-787.
(16) Ledesma, P., J. Usaola, and J. L. Rodriguez. Transient stability of a fixed speed WF. *Renewable energy* 2003; 28.9: 1341-1355.
(17) Zhang, Y., Xie, D., Feng, J., & Wang, R. Small-signal Modeling and Modal Analysis of Wind Turbine Based on Three-mass Shaft Model. *Electric Power Components and Systems*2014*;* 42(7), 693-702.
(18) Liu, L., & Xie, D. Performance comparison of two different filter design approaches for torsional vibration damping in a doubly fed induction generator-based wind turbine. *The Journal of Engineering* 2015; 1(1).
(19) Kundur, P. (1994). *Power system stability and control* (Vol. 7). N. J. Balu, & M. G. Lauby (Eds.). New York: McGraw-hill.
(20) Fan, Y., Xitian, W., Yingxin, X., & Chen, C. Dynamic Equivalence of Torsional Interaction in Multi-identical-machine Power System. *Electric Power Components and Systems* 2007; 35(5), 525-537.

Da Xie (Non-member) received his B.S. from SJTU, Shanghai, China, in 1991; his M.S. from HIT, Harbin, China, in 1996; and his Ph.D. from SJTU in 1999. His research focuses on power transmission and distribution of smart grids, and grid-connected techniques of renewable energy.

Junbo Sun (Non-member) received the B.S from Shanghai University of Electric Power, Shanghai, China, in 2013. Now, he is a postgraduate majoring in electrical engineering in SJTU, Shanghai, China. His general research interests are power system stability, control, security and wind power.

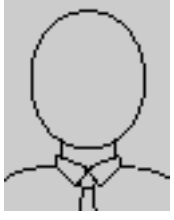

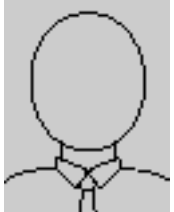

Yupu Lu (Non-member) received the B.S from Tianjin University, Tianjin, China, in 2013. Now, he is a postgraduate majoring in electrical engineering in Shanghai Jiao Tong University, Shanghai, China. His current research interests are wind power modeling and control and photovoltaic inverter.

Yucheng Lou (Non-member) received her Bachelor's degree in electrical engineering in 2008 from Shanghai Jiao Tong University (SJTU), Shanghai, China. Currently, she is pursuing a Master's degree in SJTU. Her research interests are distributed energy and wind power.

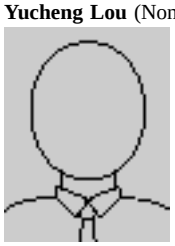

Chenghong Gu (Non-member) received the B.S and M.S. from Shanghai University of Electric Power and SJTU, Shanghai, China, in 2003 and 2007, respectively, and the Ph.D. from the University of Bath, U.K., in 2010. Now, he is a ~~KTA~~ Lecturer and EPSRC fellow in the Department of Electronic and Electrical Engineering, University of Bath. His research interests are power system planning and smart grid.

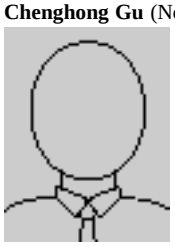

Furong Li (Non-member) received the B.Eng. degree in electrical engineering from Hohai University, China, in 1990, and the Ph.D. degree from Liverpool John Moores University, Liverpool, U.K., in 1997. Her major research interests are in the areas of power system planning, operation, automation, and power system economics.